Molecular Crystals and Liquid Crystals

ISSN: 1542-1406 (Print) 1563-5287 (Online) Journal homepage: http://www.tandfonline.com/loi/gmcl20

Synthesis and Characterization of Mesogenic Compounds Possessing Bithiophene and Benzoxazole Units

Kun Hu, Pei Chen, Xinbing Chen & Zhongwei An

To cite this article: Kun Hu, Pei Chen, Xinbing Chen & Zhongwei An (2015) Synthesis and Characterization of Mesogenic Compounds Possessing Bithiophene and Benzoxazole Units, Molecular Crystals and Liquid Crystals, 608:1, 25-37, DOI: 10.1080/15421406.2014.949593

To link to this article: http://dx.doi.org/10.1080/15421406.2014.949593

Published online: 03 Mar 2015.

Mol. Cryst. Liq. Cryst., Vol. 608: pp. 25–37, 2015

ISSN: 1542-1406 print/1563-5287 online
DOI: 10.1080/15421406.2014.949593

Synthesis and Characterization of Mesogenic Compounds Possessing Bithiophene and Benzoxazole Units

KUN HU,[1] PEI CHEN,[1] XINBING CHEN,[1,*] AND ZHONGWEI AN[1,2]

[1]Key Laboratory of Applied Surface and Colloid Chemistry (MOE), School of Materials Science and Engineering, Shaanxi Normal University, Xi'an, P R China
[2]Xi'an Modern Chemistry Research Institute, Xi'an, P R China

*A series of bithiophene-based compounds, 2-(5′-alkyl-2,2′-bithiophene-5-yl)-benzoxazole derivatives (**nTBx**), bearing different substituents (H, CH_3, Cl, NO_2) at the 5-position, were prepared and characterized. They exhibit enantiotropic mesophases with temperature ranges of 3°C–61°C and 4°C–71°C during heating and cooling, and **nTBx** with electron-withdrawing substituents (NO_2, Cl) display higher clearing temperatures and wider mesophase ranges than those of corresponding homologues with electron donating substituents. Compared to biphenyl-based analogs (**nB-x**), **nTBx** show much larger red-shifted absorption bands (374–388 nm) and photoluminescence emission peaks (453–458 nm), thereby illustrating the impact of the bithiophene core on electronic properties originating from the π-molecular orbitals.*

Keywords Benzoxazole compounds; bithiophene derivative; mesophase; photophysical property

1. Introduction

With the change of the molecular structure of calamitic liquid crystals, their mesomorphic properties differ significantly. To design novel thermotropic liquid crystals, the molecular architecture, such as suitable selection of core fragment, linking group, and terminal functionality, is considered to be primary. In general, a 1,4-disubstituted phenyl ring serves as a major mesogenic core unit for the known calamitic liquid crystals. However, with the discovery of banana type liquid crystals, attentations has been changed to the incorporation of nonlinear units in the mesogenic core. Among the nonlinear fragments, thiophene has attracted the interest of many research groups [1–10]. The incorporation of thiophene in the mesogenic core will create a bent molecular structure that substantially affects the transition temperatures, dielectric anisotropy, optic, and other properties of mesogens, in comparision with the benzenoid analogues.

*Address correspondence to X. Chen, Key Laboratory of Applied Surface and Colloid Chemistry (MOE), School of Materials Science and Engineering, Shaanxi Normal University, Xi'an 710062, P R China. Email: chenxinbing@snnu.edu.cn

Color versions of one or more of the figures in the article can be found online at www.tandfonline.com/gmcl.

On the other hand, benzoxazoles are a group of heterocyclic compounds that have been used as central cores to generate novel compounds exhibiting unique mesophases. There are some examples of benzoxazole-based mesogenic and metallo-mesogenic materials [11–21], and the formation of a mesophase in benzoxazole-based mesogens has been found to be greatly affected by polar substituents, polarisability, and intramolecular or/and intermolecular force.

Recently, we have studied series of mesogenic 2-arylbenzoxazole derivatives (**nPB-x** and **nB-x**, as shown in Fig. 1) with different polar substituents at 5-position of terminal benzoxazole unit, where the substituents with stronger electron-withdrawing properties generally give a wider mesomorphic temperature domain [18, 19]. Furthermore, via introducing two lateral fluoro substituents to biphenyl unit, the nematic mesophase as well as low melting point are achieved [20, 21].

The above mentioned results inspired us to perform a broader study of benzoxazole-based calamitic mesogens and design novel liquid crystal materials possessing bithiophene and benzoxazole units. Here, we describe the synthesis and properties of 2-(5′-alkyl-2,2′-bithiophene-5-yl)-benzoxazole derivatives (**nTBx**) containing bithiophene and benzoxazole moieties depicted in Figure 1. We focus our attentation on the relationship between molecular structure and the properties of these molecules, as well as the corresponding comparision among **nTBx**, **nPB-x** and **nB-x**.

2. Results and Discussion

2.1 Synthesis and Characterization

A synthetic route towards **nTBx** is illustrated in Scheme 1, in which alkylation of bithiophene, Vilsmeier-Haack formylation, condensation of 2-aminophenols with the corresponding bithiophene aldehydes and subsequent intramolecular cyclization were carried out in turn. It was noted that, both 2,3-dichloro-5,6-dicyanobenzoquinone (DDQ) and iodobenzene diacetate (IBD) were chosen as oxidative reagent in the intramolecular cyclization to generate benzoxazole ring skeletons, while the latter gave satisfactory results. The

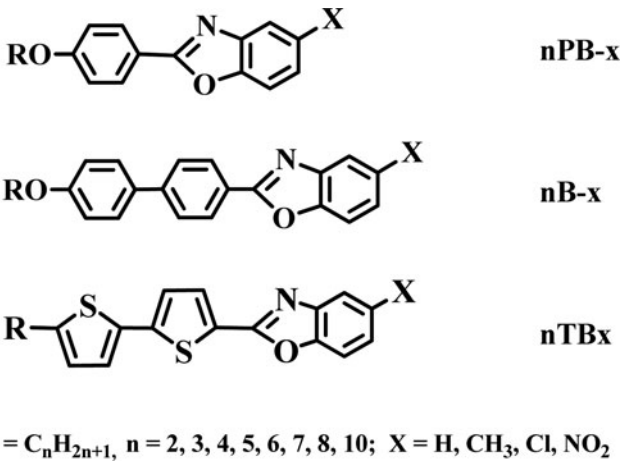

Figure 1. Structures of **nPB-x,**·**nB-x,** and **nTBx**.

bithiophene-based compounds **nTBx**, with carbon atoms in the alkyl chain from 7 to 10, and possessing polar substituents on benzoxazole moiety, were obtained in purities greater than 98% [high performance liquid chromatography (HPLC) or gas chromatography (GC)] and with overall yields of 40%–46%.

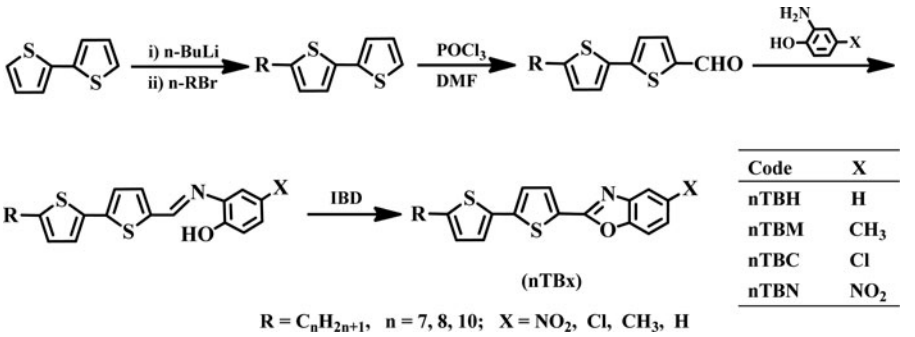

Code	X
nTBH	H
nTBM	CH_3
nTBC	Cl
nTBN	NO_2

Scheme 1. Synthesis of **nTBx**.

The structures of the products were characterized by infrared (IR), proton nuclear magnetic resonance (^{1}H-NMR), GC with electron impact-mass spectrometry (GC/EI-MS), and elemental analysis (EA). From the IR data of compound **10TBN**, the peaks at 1617, 1577, and 1501 cm^{-1} could be attributed to vibrations of the aromatic ring skeleton. It was noted that the absorption band of C=N in the benzoxazole moiety overlapped with the vibrations of the aromatic ring skeleton at 1617 cm^{-1}, and a similar phenomenon was found with compounds **nTBH**, **nTBM,** and **nTBC**. The bands at 1547 and 1344 cm^{-1} were assigned to the anti-symmetric and symmetric N−O stretching vibrations of the nitro group. In ^{1}H-NMR spectrum of **10TBN**, the peaks at 8.55, 8.28, and 7.61 ppm were assigned to the protons of phenyl ring in nitro substituted benzoxazole group. The peaks at 7.82, 7.14, and 6.74 ppm were attributed to the protons of the bithiophene ring. The proton in CH_2 group adjacent to bithiophene was assigned at 2.81 ppm, and protons in the alkyl group appeared at 0.75–2.00 ppm. In GC/EI-MS spectrum of **10BTN**, the peak of the positively charged molecular ion appeared at *m/z* 468.17 with a relative intensity of 26%, consistent with the theoretical value (468.63). EA result of **10BTN** (C 63.77, H 5.71, and N 5.90) was in accordance with the calculated data (C 64.07, H 6.02, and N 5.98). All these results confirmed the proposed structures of compounds in the **nBTx** series.

2.2 Mesomorphic Properties

Mesomorphic properties of **nTBx** were determined by differential scanning calorimetry (DSC) and polarizing optical microscopy (POM). DSC curves obtained under similar conditions overlapped one another, confirming the reproducibility of the measurements. The phase transition temperatures reported in the present paper were the peak values of the transition on the DSC curves. Phase identification was made by comparing the observed textures with those reported in the literature. Clear-cut transition temperatures and textures were obtained from DSC and POM observations for all the compounds, and were in good agreement with each other for the multiple heating/cooling cycles. The phase transition temperatures, the associate enthalpy changes and mesophase textures of the **nTBx** are summarized in Table 1. Due to the fact that the sliver-coated cell was corrupted during DSC

Table 1. Types of phase transition, temperatures and corresponding enthalpies obtained by POM and DSC methods for compounds **nTBH**, **nTBM**, **nTBC,** and **nTBN**

	Transition temperature, °C (enthalpy change/kJ mol^{-1})	
Compounds	Heating process	Cooling process
7TBH	Cr 105.8 (23.6) I	I 86.8 (–24.3) Cr
8TBH	Cr 105.5 (35.3) I	I 87.4 (–36.9) Cr
10TBH	Cr 105.4 (30.4) I	I 85.6 (–33.0) Cr
7TBM	Cr 87.7 (20.2) N 93.9 (0.2) I	I 90.8 (–0.4) N 76.9 (–1.4) SmC 60.8 (–16.7) Cr
8TBM	Cr 88.5 (14.1) SmC 92.6 (7.5) I	I 87.7 (–0.7) N 82.1 (–3.5) SmC 64.3 (–22.0) Cr
10TBM	Cr 81.7 (19.9) SmC 95.7 (3.7) I	I 91.8 (–4.2) SmC 62.4 (–18.0) Cr
7TBC*	Cr 73.5 SmC 134.0 I	I 133.0 SmC 67.0 Cr
8TBC*	Cr 94.0 SmC 135.0 I	I 134.7 SmC 63.5 Cr
10TBC*	Cr 91.4 SmC 134.5 I	I 134.2 SmC 66.6 Cr
7TBN	Cr 145.0 (9.2) SmC 147.9 (1.0) I	I 144.9 (–2.5) SmC 141.0 (–12.6) Cr
8TBN	Cr 145.3 (8.5) SmC 150.3 (1.7) I	I 146.3 (–2.4) SmC 140.3 (–9.5) Cr
10TBN	Cr 142.5 (9.6) SmC 152.5 (2.9) I	I 148.4 (–2.9) SmC 137.8 (–10.0) Cr

Note: *, data obtained by POM; Cr: crystal; SmC: smectic C mesophase; N: nematic mesophase; I: isotropic liquid.

measurement on samples in **nTBC** series, the phase transition temperatures and mesophase textures were in these cases determined only by POM.

As shown in Table 1, the compounds **nTBx** exhibited enantiotropic smectic mesophases for alky chain lengths of 7 to 10 carbons with exception of **nTBH**. The phases of **7TBM**, **7TBC**, and **10TBN** were assigned from the typical focal conic textures and Schlieren textures during both heating and cooling, respectively, as shown in Fig. 2. Compared to other series, **nTBH** showed no mesophase at all whether with short or long terminal alkyl chain during both heating and cooling processes, which indicated that the substituents (NO_2, CH_3, and Cl) at benzoxazole moiety were helpful to increase the mesophase stability of bithiophene-based compounds. This was in accordance with the reported results for compounds **nPB-x** and **nB-x** [18, 19].

Compared to biphenyl-based analogs **nB-x**, bithiophene groups in compounds **nTBx** were observed to lower the corresponding melting point and the stability of mesophase, as shown in Table 1 and Fig. 3, which was attributed to its nonlinear conformations resulting from the bithiophene structure. It is obvious that, compared to **nPB-x**, bithiophene-based analogs **nTBx** exhibited slightly higher the melting point due to its longer mesogenic core.

2.3 Thermal Stability

As shown in Fig. 4a, the TGA curves of the samples **10TBx** series were recorded at 30°C–600°C under a nitrogen atmosphere. It can be seen that compounds **10TBH**, **10TBM**, and **10TBC** showed the onset of decomposition at 250°C, 235°C, and 260°C, respectively,

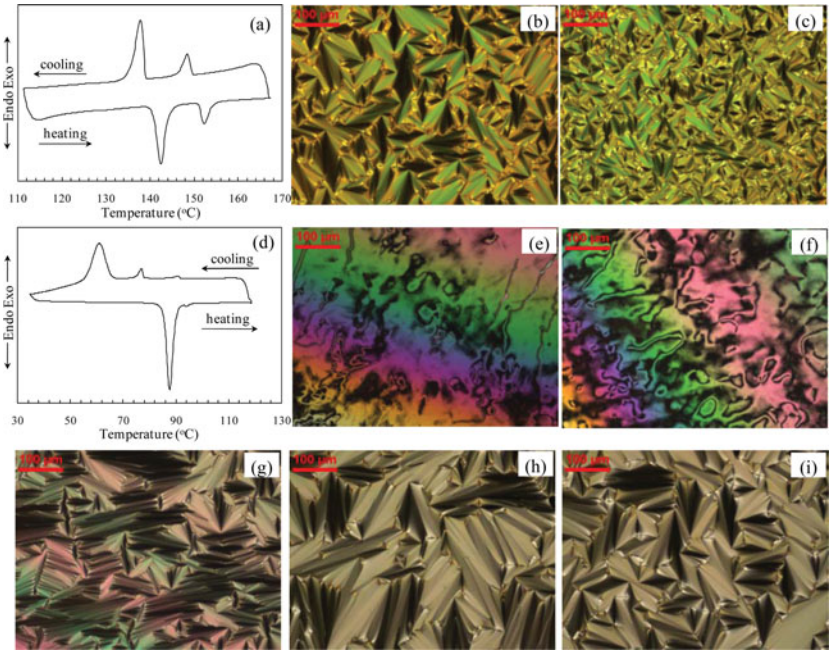

Figure 2. DSC traces and photomicrographs (×200) of **10TBN** (a, b, c), **7TBM** (d, e, f, g), and **7TBC** (h, i); focal conic texture of the smectic mesophase at 146°C (b), 120°C (h) on heating and 145°C (c), 70°C (g), 111°C (i) on cooling; Schlieren texture of the nematic mesophase at 90°C (e) on heating and 87°C (f) on cooling.

and became almost completely decomposed until 360°C. On the other hand, **10TBN** exhibited a one-step decomposition starting at 260°C, and more than 70 wt% had decomposed within the temperature range 260–480°C. This indicated that the strongly polar nitro-substituent in **nTBN** increased the dipole–dipole interaction between the molecules, giving greater thermal stability.

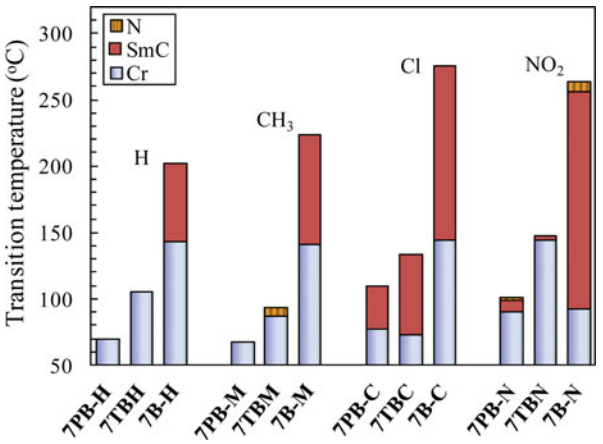

Figure 3. The transition temperatures of series **7TBx**, **7B-x,** and **7PB-x**.

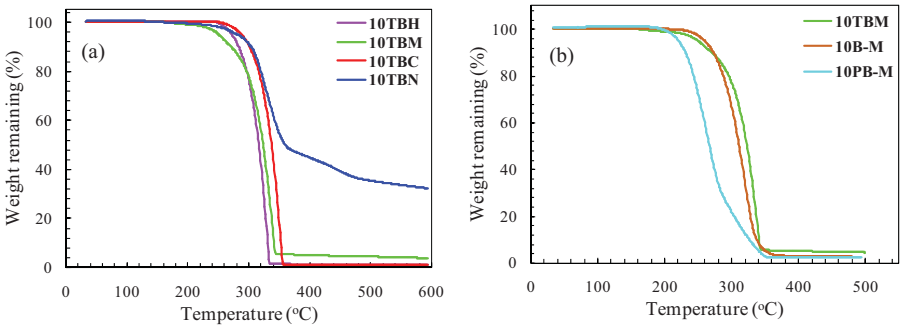

Figure 4. TGA curves of compounds **10TBx** (a), series **10TBM**, **10B-M,** and **10PB-M** (b).

Among the analogs **nTBx**, **nB-x**, and **nPB-x**, **nTBx**, and **nB-x** exhibited comparable high thermal stability, whereas **nPB-x** gave the lowest thermal stability. As shown in Fig. 4b, **10TBM** and **10B-M** exhibited the high onset of decomposition at 235°C, which was attributed to their high π-π conjugation between the aromatic rings. **10PB-M** displayed the lowest onset of decomposition at 185°C due to its lowest π-π conjugation derived from the smallest mesogenic core.

2.4 The Effects of Alkyl Chain and Polar Substituents on Liquid Crystalline Properties

In general, the length of the alkyl chain had an influence, not only on the nature of the mesophases but also on the mesomorphic temperature ranges. An increase in terminal length resulted in enhanced dipole–dipole interaction between the terminal chains, leading to an increase in stability of the mesophases in rod-like mesogens. Figure 5 and Table 1 illustrate the transition temperatures of compounds **nTBx**. It was found that, with the increase of the carbon numbers (*n*) in the alkyl chain, the mesomorphic temperature domains varied from 4°C to 14°C and 23°C to 30°C during heating and cooling for **nTBM**, 41°C to 61°C and 66°C

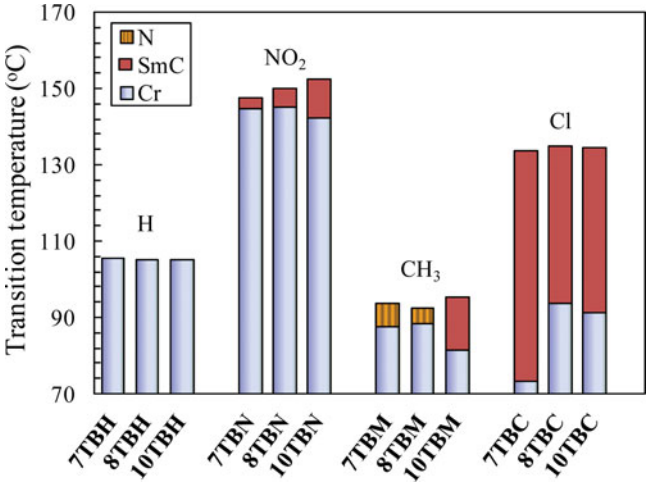

Figure 5. The transition temperatures of compounds **nTBx** during heating.

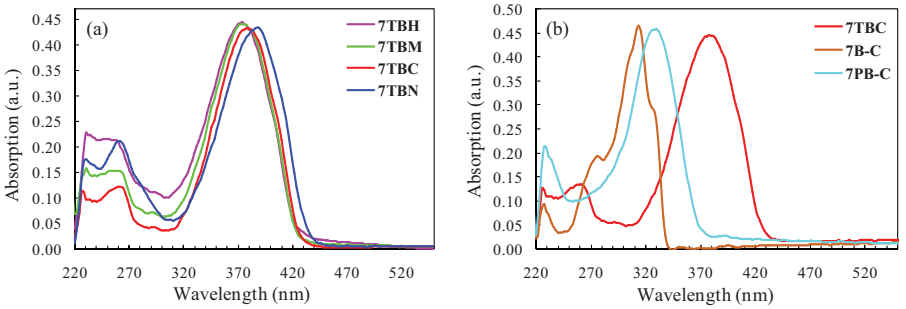

Figure 6. UV spectra of compounds **7TBx** (a) and series **7TBC**, **7B-C,** and **7PB-C** (b) in CH_2Cl_2 (1.0×10^{-5} mol L^{-1}).

to 71°C for **nTBC**, 3°C to 10°C and 4°C to 11°C for **nTBN**, respectively. Both the melting points and clearing points of **nTBx** displayed slightly increasing/decreasing tendency in ascending homologues. Compared to biphenyl-based **nB-x**, the narrower mesophase range of **nTBx** was attributed to its non-linear conformations resulting from the bithiophene structure.

The polar substitutes had an influence, not only on the mesophase ranges but also on the clearing points. Compounds **nTBx** with electron-withdrawing substituents (NO_2, Cl) displayed higher clearing temperatures (T_{cl}) than those of corresponding homologues with electron donating substituents (Fig. 5 and Table 1), and the higher T_{cl} being attributed to enhanced conjugative interaction, which was consistent with the literature results [16, 18–20]. Substituents with a stronger electron-withdrawing effect led to a wider mesomorphic temperature domain with benzoxazole-based liquid crystals, due to the stronger dipole–dipole interaction between the molecules. In the case of bithiophene-based compounds **nTBx**, the effect of substituents on the mesophase range varied in the order of Cl > NO_2 > CH_3 > H, which was slightly different to that in **nB-x** and **nPB-x** (NO_2 > Cl > CH_3 > H).

2.5 Photophysical Properties

The absorption spectra of compounds **7TBx** recorded in methylene chloride are shown in Fig. 6a. All the compounds exhibited a broad absorption band (λ_{max} = 374 nm for

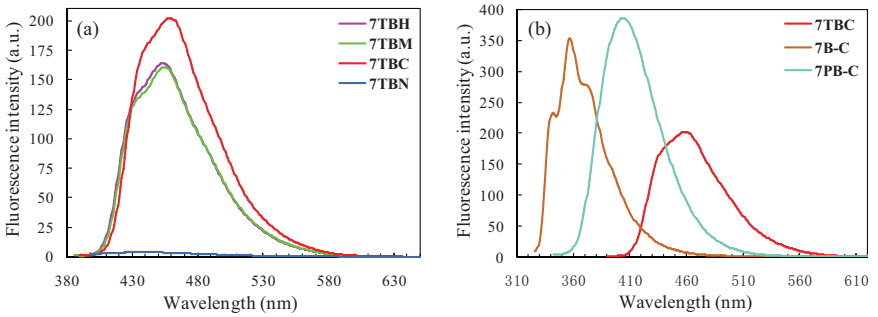

Figure 7. Emission spectra of compounds **7TBx** (a) and series **7TBC**, **7B-C**, and **7PB-C** (b) in CH_2Cl_2 (2.0×10^{-7} mol L^{-1}).

7TBH, 374 nm for **7TBM**, 378 nm for **7TBC**, and 388 nm for **7TBN**) attributable to the electronic transition originating from the π-molecular orbitals. The absorption bands of the substituted compounds (**7TBM**, **7TBC**, and **7TBN**) were red-shifted compared with that of the non-substituted compound **7TBH**, illustrating the impact of substituent groups on electronic properties.

Compared to **nB-x** and **nPB-x**, the bithiophene-based analogs **nTBx** showed a much larger red-shifted absorption band, as shown in Fig. 6b, which were attributed to the increase in the strength of π-conjugation resulting from the more stable planar conformation of the bithiophene structure. It is known that adjacent phenyl groups will adapt a nonplanar twisted conformation [22], so the molecular structures containing bithiophene instead of biphenyl groups will result in planar conformation, giving rise to extensive intramolecular conjugation [23, 24].

The fluorescence spectra of compounds **7TBx** are shown in Fig. 7a, where the nitro substituent (**7TBN**) let to a significantly decrease in emission, a common phenomenon in nitro-substituted fluorophores. Apart of **7TBN**, these compounds exhibited intense photoluminescence emission at low concentration (2.0×10^{-7} molL^{-1}) in CH_2Cl_2 solutions when they were excited at their absorption maxima, in which the emission bands appeared at 453 nm (**7FBH**), 455 nm (**7FBM**), and 458 nm (**7FBC**), respectively. Compared to **nB-x** and **nPB-x**, the corresponding bithiophene-based analogs **nTBx** showed much larger red-shifted emission peaks, as shown in Fig. 7b, which was consistent with the trend observed in the absorption spectra (Fig. 6b).

3. Conclusions

In summary, 2-(5′-alkyl-2,2′-bithiophene-5-yl)-benzoxazole derivatives **nTBx** were designed and synthesized. Among the **nTBx** series, **nTBN**, **nTBM,** and **nTBC** exhibited smectic mesomorphic phases, whereas **nTBH** gave no mesophase at all. The bithiophene-based analogs **nTBx** showed comparable mesophase range compared with **nPB-x**, and comparable thermal stability but lower melting points compared with **nB-x**. The substituents had an obvious effect on the UV absorption bands of **nTBx** in the sequence of $NO_2 > Cl > CH_3 > H$. Compared to **nPB-x** and **nB-x**, **nTBx** showed much larger red-shifted absorption bands and photoluminescence emission peaks, which was attributed to the increase in the strength of π-conjugation resulting from the more stable planar conformation of the bithiophene structure.

4. Experimental

4.1 Materials

Bithiophene, alkyl bromide, ammonium chloride, butyl lithium, phosphorus oxychloride, IBD, 2-aminophenol, 2-amino-4-nitrophenol, 2-amino-4-chlorophenol, and 2-amino-4 - methylphenol were purchased from Aladdin-reagent Co. (Shanghai, China) and used as received. Tetrahydrofuran, silica gel, N,N-dimethylformamide (DMF), petroleum ether (PE), ethyl acetate (EA), hexane, absolute ethanol, chloroform, and anhydrous potassium carbonate were purchased from Sinopharm Chemical Reagent Co. (Shanghai, China). Chloroform was dehydrated by pre-dried 4Å molecular sieves which were activated at 350°C for 4 h prior to use.

4.2 Characterization and Measurements

The structures of the final products and intermediates were confirmed by a variety of spectral methods. IR spectra were recorded on a Nicolet Avatar360E spectrometer (Thermo Electron Corporation, Madison, Wis., USA). ^{1}H-NMR spectra, with tetramethylsilane (TMS) as internal standard, were recorded on a Bruker AV 300 (300 MHz) instruments (Bruker Corporation, Karlsruhe, Germany). The mass spectra were obtained by GC/EI-MS Thermo DSQ II (Thermo Finnigan, CA, USA) with *m/z* 50 to 650. EA was performed for C, H, and N in an Elementar Vario EL III instrument (Elementar Analysensysteme GmbH, Hanau, Germany). The phase transition temperatures were measured by DSC, Shimatsu DSC-60 (Shimadzu Corporation, Kyoto, Japan) in nitrogen at a heating and cooling rate of 5°C min^{-1}, and POM, LEICA DM2500P (Leica Microsystems GmbH, Wetzlar, Germany) with Linkam THMS600 hot-stage (Linkam Scientific Instruments Ltd., Tadworth, UK) and control unit at a heating and cooling rate of 0.5°C min^{-1}. Thermogravimetric analysis (TGA) was carried out with a TA Q50 (TA Instruments, New Castle, DE, USA) in nitrogen (flow rate: 100 cm^3 min^{-1}) at a heating rate of 10°C min^{-1}. UV-vis absorption spectra were recorded using a Hitachi U-3900UV spectrometer (Hitachi High-Technologies Corporation, Tokyo, Japan). The emission spectra were determined using a Hitachi F-7000 spectrometer (Varian Ltd., Madrid, Spain).

4.3 Synthesis

As an example, the preparation procedure of 2-(5′-decyl-2,2′-bithiophene-5-yl)-5-nitrobenzoxazole (**10TBN**) is described below.

4.3.1 Synthesis of 5-decyl-2,2′-bithiophene. Under nitrogen protection, 2.5 M butyl lithium (26 mL, 66 mmol) was injected into a cooled (−78°C), stirred solution of bithophene (60 mmol) in THF (150 mL). After addition, the reaction temperature was maintained at −78°C for 1 h, followed by the addition of solution of n-decyl bromide (66 mmol) in THF (25 mL). Then, the system was kept at −78°C for 1 h after addition, and allowed to warm to room temperature overnight. After addition of 150 mL of saturated solution of ammonium chloride, EA was added for three extraction cycles. The combined organic extracts were washed with water (100 mL), dried with magnesium sulfate, and then the solvent was removed in vacuo. The residue was purified via column chromatography on silica gel using hexane as eluent to give purity above 98% for GC measurement. Yellow liquid was obtained with yield of 65%.

4.3.2 Synthesis of 5-decyl-2,2′-bithiophene-5′-carboxaldehyde. Under nitrogen protection, 12.24 g phosphorus oxychloride (80 mmol) was dropped into a cooled (0°C–5°C), stirred solution of DMF (80 mL). After addition, the reaction temperature was maintained below 5°C for 0.5 h, followed by the addition of solution of 5-decyl-2,2′-bithiophene (20 mmol) in DMF (20 mL). Then, the system was stirred at 80°C for 5 h. After the mixture was cooled to room temperature, the system was diluted with water. A 10% aqueous solution of potassium carbonate (100 mL) was added to adjust ph value to neutral, and the mixture was extracted with EA for three times. The combined organic extracts were washed with water (100 mL), dried over magnesium sulfate and the solvent was removed in vacuo. The residue was purified via column chromatography on silica gel using PE/EA (8/1) as eluent to give purity above 98% for GC measurement. Yellow crystals were obtained with yield of 85%; m.p. 44.9°C−45.4°C.

*4.3.3 Synthesis of 2-(((5′-decyl-2,2′-bithiophene-5-yl)methylene)amino)-4-nitrophenol (**10TSN**).* To a 100 mL, round-bottom flask equipped with an overhead stirrer and condenser, 0.74 g of 5-decyl-2,2′-bithiophene-5′-carboxaldehyde (2.2 mmol), 0.51 g of 2-amino-4-nitrophenol (3.3 mmol) and 25 mL of ethanol were added. The reaction system was stirred at reflux for 6 h. After the mixture was cooled to room temperature, it was filtrated through Celite. The solid was washed with 15 mL of ethanol for several times to give purity above 98% (HPLC). Pale yellow crystals were obtained with yield of 90%; m.p. 141.2°C −141.6°C.

*4.3.4 Synthesis of 2-(5′-decyl-2,2′-bithiophene-5-yl)-5-nitrobenzoxazole (**10TBN**).* To a 100 mL round-bottom flask equipped with an overhead stirrer and condenser, 0.50 g of **10TSN** (1.07 mmol), 0.43 g of IBD (1.32 mmol), and 50 mL of anhydrous chloroform. The reaction system was stirred at reflux for 6 h. After completion of the reaction, the mixture was diluted with water and extracted with chloroform for three times. The combined organic phase was dried over magnesium sulfate. After removal of the solvent in vacuo, the residue was purified via column chromatography on silica gel using PE/EA (8/1) as eluent to give purity above 98% for HPLC measurement. Pale yellow crystals were obtained with yield of 76%; m.p. 143°C.

^{1}H-NMR (300 MHz, $CDCl_3$, TMS): δ (ppm) 8.55 (d, $J = 2.1$ Hz, 1H), 8.28 (q, $^3J = 9.0$ Hz, $^4J = 2.1$ Hz, 1H), 7.82 (d, $J = 3.9$ Hz, 1H), 7.61 (d, $J = 8.7$ Hz, 1H), 7.14 (t, $J = 3.0$ Hz, 2H), 6.74 (d, $J = 3.3$ Hz, 1H), 2.81 (t, $J = 7.5$ Hz, 2H), 1.69 (m, 2H), 1.27 (m, 14H), 0.88 (t, $J = 6.6$ Hz, 3H).

IR (KBr, pellet, cm^{-1}): 3100, 3071, 3037, 2954, 2918, 2850, 1617, 1577, 1547, 1528, 1501, 1467, 1438, 1344, 1309, 1267, 1235, 1062, 997, 882, 831, 799, 738, 716, 690.

EI-MS m/z (rel. int.): 468.17 (M^+, 26), 341.01 (100), 295.05 (34).

EA: Calc. for $C_{25}H_{28}N_2O_3S_2$: C 64.07, H 6.02, N 5.98; Found: C 63.77, H 5.71, N 5.90.

The other bithiophene-based compounds (**nTBx**) were prepared using a similar procedure.

7TBH: Pale yellow crystals, yield 74%; m.p. 106°C.

^{1}H-NMR (300MHz, $CDCl_3$, TMS): δ (ppm) 7.77 (d, $J = 3.9$ Hz, 1H), 7.71 (m, 1H), 7.52 (m, 1H), 7.32 (m, 2H), 7.12 (q, $^3J = 6.3$ Hz, $^4J = 3.9$ Hz, 2H), 6.72 (d, $J = 3.3$ Hz, 1H), 2.80 (t, $J = 7.5$ Hz, 2H), 1.69 (m, 2H), 1.34–1.29 (m, 8H), 0.89 (t, $J = 6.6$ Hz, 3H).

IR (KBr, pellet, cm^{-1}): 3071, 2957, 2921, 2850, 1614, 1574, 1550, 1507, 1447, 1239, 1071, 1007, 873, 810, 792, 743, 715, 502.

EI-MS m/z (rel. int.): 381.11 (M^+, 31), 296.01 (100), 176.97 (3), 147.98 (2).

EA: Calc. for $C_{22}H_{23}NOS_2$: C 69.25, H 6.08, N 3.67; Found: C 69.06, H 5.79, N 3.68.

8TBH: Pale yellow crystals, yield 73%; m.p. 105°C.

^{1}H-NMR (300 MHz, $CDCl_3$, TMS): δ (ppm) 7.78 (d, $J = 3.6$ Hz, 1H), 7.72 (m, 1H), 7.52 (m, 1H), 7.34 (m, 2H), 7.12 (q, $^3J = 6.3$ Hz, $^4J = 3.6$ Hz, 2H), 6.73 (t, $J = 3.3$ Hz, 1H), 2.83 (t, $J = 7.5$ Hz, 2H), 1.69 (m, 2H), 1.28 (m, 10H), 0.88 (t, $J = 6.6$ Hz, 3H).

IR (KBr, pellet, cm^{-1}): 3072, 2955, 2921, 2850, 1614, 1575, 1508, 1446, 1240, 1073, 1009, 796, 744.

EI-MS m/z (rel. int.): 395.11 (M^+, 30), 296.00 (100), 177.01 (5), 147.92 (3).

EA: Calc. for $C_{23}H_{25}NOS_2$: C 69.83, H 6.37, N 3.54; Found: C 69.76, H 6.36, N 3.54.

10TBH: Pale yellow crystals, yield 73%; m.p. 105°C.

^{1}H-NMR (300 MHz, $CDCl_3$, TMS): δ (ppm) 7.77 (d, $J = 3.9$ Hz, 1H), 7.71 (m, 1H), 7.52 (m, 1H), 7.33 (m, 2H), 7.12 (q, $^3J = 6.3$ Hz, $^4J = 3.9$ Hz, 2H), 6.72 (d, $J = 3.3$ Hz, 1H), 2.80 (t, $J = 7.5$ Hz, 2H), 1.69 (m, 2H), 1.27 (m, 14H), 0.88 (t, $J = 6.3$ Hz, 3H).

IR (KBr, pellet, cm^{-1}): 3090, 3073, 2954, 2920, 2849, 1614, 1575, 1552, 1508, 1469, 1452, 1444, 1384, 1240, 1073, 1009, 999, 876, 811, 796, 759, 743.

EI-MS m/z (rel. int.): 423.18 (M^+, 43), 296.00 (100), 176.99 (3), 148.09 (3).

EA: Calc. for $C_{25}H_{29}NOS_2$: C 70.88, H 6.90, N 3.31; Found: C 70.51, H 6.59, N 3.31.

7TBM: Pale yellow crystals, yield 75%; m.p. 88°C.

^{1}H-NMR (300 MHz, $CDCl_3$, TMS): δ (ppm) 7.74 (d, $J = 3.6$ Hz, 1H), 7.49(s, 1H), 7.39 (d, $J = 8.4$ Hz, 1H), 7.11 (m, 3H), 6.72 (d, $J = 3.3$ Hz, 1H), 2.80 (t, $J = 7.5$ Hz, 2H), 2.46 (s, 3H), 1.69 (m, 2H), 1.34 – 1.29 (m, 8H), 0.89 (t, $J = 6.9$ Hz, 3H).

IR (KBr, pellet, cm^{-1}): 2954, 2924, 2849, 1612, 1572, 1547, 1511, 1468, 1438, 1425, 1257, 1193, 1058, 1017, 875, 821, 797, 786, 709.

EI-MS m/z (rel. int.): 395.08 (M^+, 34), 310.04 (100), 177.03 (6).

EA: Calc. for $C_{23}H_{25}NOS_2$: C 69.83, H 6.37, N 3.54; Found: C 69.68, H 6.18, N 3.55.

8TBM: Pale yellow crystals, yield 75%; m.p. 88°C.

^{1}H-NMR (300 MHz, $CDCl_3$, TMS): δ (ppm) 7.74 (d, $J = 3.9$ Hz, 1H), 7.48 (s, 1H), 7.39 (d, $J = 8.1$ Hz, 1H), 7.11 (m, 3H), 6.72 (d, $J = 3.6$ Hz, 1H), 2.80 (t, $J = 7.5$ Hz, 2H), 2.46 (s, 3H), 1.68 (m, 2H), 1.28 (m, 10H), 0.88 (t, $J = 6.6$ Hz, 3H).

IR (KBr, pellet, cm^{-1}): 2953, 2921, 2851, 1618, 1579, 1547, 1505, 1468, 1443, 1262, 1069, 1000, 874, 801, 783, 717.

EI-MS m/z (rel. int.): 409.13 (M^+, 49), 310.00 (100), 177.00 (5).

EA: Calc. for $C_{24}H_{27}NOS_2$: C 70.37, H 6.64, N 3.42; Found: C 70.09, H 6.40, N 3.41.

10TBM: Pale yellow crystals, yield 76%; m.p. 82°C.

^{1}H-NMR (300 MHz, $CDCl_3$, TMS): δ (ppm) 7.74 (d, $J = 3.9$ Hz, 1H), 7.49 (s, 1H), 7.39 (d, $J = 8.4$Hz, 1H), 7.11 (m, 3H), 6.72 (d, $J = 3.3$ Hz, 1H), 2.80 (t, $J = 7.5$ Hz, 2H), 2.46 (s, 3H), 1.68 (m, 2H), 1.26 (m, 14H), 0.88 (t, $J = 6.3$ Hz, 3H).

IR (KBr, pellet, cm^{-1}): 2953, 2920, 2850, 1617, 1579, 1547, 1505, 1481, 1468, 1443, 1429, 1262, 1068, 1001, 874, 801, 716.

EI-MS m/z (rel. int.): 437.17 (M^+, 73), 310.03 (100), 176.97 (3).

EA: Calc. for $C_{26}H_{31}NOS_2$: C 71.35, H 7.14, N 3.20; Found: C 71.05, H 6.90, N 3.16.

7TBC: Pale yellow crystals, yield 71%; m.p. 74°C.

^{1}H-NMR (300 MHz, $CDCl_3$, TMS): δ (ppm) 7.76 (d, $J = 3.9$ Hz, 1H), 7.67 (d, $J = 1.8$ Hz, 1H), 7.44 (d, $J = 8.4$ Hz, 1H), 7.29 (q, $^3J = 8.4$ Hz, $^4J = 1.8$ Hz, 1H), 7.13 (t, $J = 3.9$ Hz, 2H), 6.72 (d, $J = 3.6$ Hz, 1H), 2.80 (t, $J = 7.5$ Hz, 2H), 1.69 (m, 2H), 1.34 – 1.29 (m, 8H), 0.89 (t, $J = 6.6$ Hz, 3H).

IR (KBr, pellet, cm^{-1}): 2956, 2924, 2849, 1605, 1566, 1545, 1509, 1469, 1449, 1422, 1384, 1258, 1192, 1060, 1017, 808, 796, 708.

EI-MS m/z (rel. int.): 415.09 (M^+, 39), 329.96 (100), 295.11 (2), 176.99 (6).

EA: Calc. for $C_{22}H_{22}ClNOS_2$: C 63.52, H 5.33, N 3.37; Found: C 63.51, H 5.18, N 3.37.

8TBC: Pale yellow crystals, yield 73%; m.p. 94°C.

^{1}H-NMR (300 MHz, $CDCl_3$, TMS): δ (ppm) 7.75 (d, $J = 3.9$ Hz, 1H), 7.66 (d, $J = 2.1$ Hz, 1H), 7.43 (d, $J = 8.7$ Hz, 1H), 7.28 (q, $^3J = 8.7$ Hz, $^4J = 2.1$ Hz, 1H), 7.11 (t, $J = 3.6$ Hz, 2H), 6.72 (d, $J = 3.6$ Hz, 1H), 2.80 (t, $J = 7.5$ Hz, 2H), 1.69 (m, 2H), 1.28 (m, 10H), 0.88 (t, $J = 6.9$ Hz, 3H).

IR (KBr, pellet, cm^{-1}): 2956, 2921, 2850, 1612, 1572, 1547, 1504, 1467, 1445, 1423, 1255, 1070, 1054, 1000, 920, 871, 802, 781, 715.

EI-MS m/z (rel. int.): 429.11 (M^+, 42), 329.96 (100), 295.03 (3), 177.02 (4).

EA: Calc. for $C_{23}H_{24}ClNOS_2$: C 64.24, H 5.63, N 3.26; Found: C 63.78, H 5.41, N 3.25.

10TBC: Pale yellow crystals, yield 74%; m.p. 91°C.

^{1}H-NMR (300 MHz, $CDCl_3$, TMS): δ (ppm) 7.75 (d, $J = 3.9$ Hz, 1H), 7.66 (d, $J = 1.8$ Hz, 1H), 7.43 (d, $J = 8.4$ Hz, 1H), 7.28 (q, $^3J = 8.4$ Hz, $^4J = 1.8$ Hz, 1H), 7.11 (t, $J = 3.6$ Hz, 2H), 6.72 (d, $J = 3.6$ Hz, 1H), 2.80 (t, $J = 7.5$ Hz, 2H), 1.68 (m, 2H), 1.26 (m, 14H), 0.88 (t, $J = 6.9$ Hz, 3H).

IR (KBr, pellet, cm^{-1}): 2957, 2920, 2849, 1611, 1572, 1547, 1504, 1468, 1444, 1424, 1256, 1070, 1051, 1001, 920, 871, 803, 783, 716, 702.

EI-MS m/z (rel. int.): 457.17 (M^+, 38), 329.95 (100), 294.99 (3), 177.02 (5).

EA: Calc. for $C_{25}H_{28}ClNOS_2$: C 65.55, H 6.16, N 3.06; Found: C 65.57, H 5.97, N 3.07.

7TBN: Pale yellow crystals, yield 75%; m.p. 145°C.

^{1}H-NMR (300 MHz, $CDCl_3$, TMS): δ (ppm) 8.55 (d, $J = 1.8$ Hz, 1H), 8.27 (q, $^3J = 8.7$ Hz, $^4J = 2.1$ Hz, 1H), 7.82 (d, $J = 3.9$ Hz, 1H), 7.61 (d, $J = 8.7$ Hz, 1H), 7.15 (d, $J = 3.3$ Hz, 2H), 6.74 (d, $J = 3.3$ Hz, 1H), 2.81 (t, $J = 7.5$ Hz, 2H), 1.70 (m, 2H), 1.35–1.30 (m, 8H), 0.89 (t, $J = 6.6$ Hz, 3H).

IR (KBr, pellet, cm^{-1}): 3099, 3070, 2955, 2925, 2849, 1616, 1577, 1546, 1527, 1500, 1467, 1438, 1343, 1309, 1268, 1237, 1059, 995, 883, 806, 792, 739.

EI-MS m/z (rel. int.): 426.13 (M^+, 49), 340.96 (100), 295.00 (32).

EA: Calc. for $C_{22}H_{22}N_2O_3S_2$: C 61.95, H 5.20, N 6.57; Found: C 61.70, H 5.01, N 6.48.

8TBN: Pale yellow crystals, yield 73%; m.p. 145°C.

^{1}H-NMR (300 MHz, $CDCl_3$, TMS): δ (ppm) 8.54 (d, $J = 2.1$ Hz, 1H), 8.27 (q, $^3J = 8.7$ Hz, $^4J = 1.5$ Hz, 1H), 7.81 (d, $J = 3.9$ Hz, 1H), 7.60 (d, $J = 8.7$ Hz, 1H), 7.14 (d, $J = 2.1$ Hz, 2H), 6.73 (d, $J = 3.0$ Hz, 1H), 2.81 (t, $J = 7.2$ Hz, 2H), 1.69 (m, 2H), 1.28 (m, 10H), 0.88 (t, $J = 6.3$ Hz, 3H).

IR (KBr, pellet, cm^{-1}): 3014, 2956, 2924, 2853, 1618, 1577, 1526, 1502, 1466, 1439, 1402, 1345, 1258, 1059, 996, 881, 808, 793, 735.

EI-MS m/z (rel. int.): 440.16 (M^+, 30), 341.00 (100), 295.00 (44).

EA: Calc. for $C_{23}H_{24}N_2O_3S_2$: C 62.70, H 5.49, N 6.36; Found: C 62.63, H 5.24, N 6.31.

Funding

The authors would like to thank the National Science Foundation Committee of China (50802058, 51373092), Key Technologies R&D Program of Shaanxi Province (2012K08-09, 2014K10-06), Natural Science Foundation of Shaanxi Province (2012JM2002, 2014JM7270), Specialized Research Fund for the Doctoral Program of Higher Education (20130202120010), Program for Changjiang Scholars and Innovative Research Team in University (IRT1070) and the Fundamental Research Funds for the Central Universities (GK201302036, GK201302037) for financial support of this work.

References

[1] Campbell, N. L., Duffy, W. L., Thomas, G. I., Wild, J. H., Kelly, S. M., *et al.* (2002). *J. Mater. Chem.*, *12*, 2706.

[2] Sharma, S., Lacey, D., & Wilson, P. (2003). *Liq. Cryst.*, *30*, 451.

[3] Getmanenko, Y. A., Kang, S.-W., Shakya, N., Pokhrel, C., Bunge, S. D., *et al.* (2014). *J. Mater. Chem. C*, *2*, 256.

[4] Cheng, X., Gao, H., Tan, X., Yang, X., Prehm, M., *et al.* (2013). *Chem. Sci.*, *4*, 3317.

[5] Bu, W., Gao, H., Tan, X., Dong, X., Cheng, X., *et al.* (2013). *Chem. Commun.*, *49*, 1756.
[6] Beneduci, A., Cospito, S., Crispini, A., Gabriele, B., Nicoletta, F. P., *et al.* (2013). *J. Mater. Chem. C*, *1*, 2233.
[7] Geese, K., Prehm, M., & Tschierske, C. (2010). *J. Mater. Chem.*, *20*, 9658.
[8] Narasimhaswamy, T., Somanathan, N., Lee, D. K., & Ramamoorthy, A. (2005). *Chem. Mater.*, *17*, 2013.
[9] Didane, Y., Videlot-Ackermann, C., Brisset, H., Ackermann, J., Raynal, P., *et al.* (2009). *Mol. Cryst. Liq. Cryst.*, *507*, 178.
[10] Byron, D., Matharu, A., Wilson, R., & Wright, G. (1995). *Mol. Cryst. Liq. Cryst.*, *265*, 61.
[11] Lai, C. K., Liu, H.-C., Li, F.-J., Cheng, K.-L., & Sheu, H.-S. (2005). *Liq. Cryst.*, *32*, 85.
[12] Majumdar, K. C., Ghosh, T., Rao, D. S. S., & Prasad, S. K. (2011). *Liq. Cryst.*, *38*, 625.
[13] Majumdar, K. C., Ghosh, T., & Shyam, P. K. (2011). *Liq. Cryst.*, *38*, 567.
[14] Majumdar, K. C., Ghosh, T., Rao, D. S. S., & Prasad, S. K. (2013). *Liq. Cryst.*, *40*, 305.
[15] Wang, H.-C., Wang, Y.-J., Hu, H.-M., Lee, G.-H., & Lai, C. K. (2008). *Tetrahedron*, *64*, 4939.
[16] Chen, C.-J., Wang, I.-W., Sheu, H.-S., Lee, G.-H., & Lai, C. K. (2011). *Tetrahedron*, *67*, 8120.
[17] Wang, C.-S., Wang, I.-W., Cheng, K.-L., & Lai, C. K. (2006). *Tetrahedron*, *62*, 9383.
[18] Chen, P., Xu, Y., Du, W., Zhang, G., Chen, X., *et al.* (2014). *Mol. Cryst. Liq. Cryst.*, DOI: 10.1080/15421406.2013.837997.
[19] Xu, Y., Chen, X., Zhao, F., Fan, X., Chen, P., *et al.* (2013). *Liq. Cryst.*, *40*, 197.
[20] Xu, Y., Hu, K., Chen, P., Gao, A., Du, W., *et al.* (2014). *Liq. Cryst.*, *41*, 1042.
[21] Hu, K., Xu, Y., Chen, P., Gao, A., Du, W., *et al.* (2014). *Liq. Cryst.*, *41*, 1455.
[22] van Eijck, L., Johnson, M. R., & Kearley, G. R. (2003). *J. Phys. Chem. A*, *107*, 8980.
[23] Guha, S., Graupner, W., Resel, R., Chandrasekhar, M., Chandrasekhar, H. R., *et al.* (1999). *Phys. Rev. Lett.*, *82*, 3625.
[24] Hong, S. Y., Kim, D. Y., & Kim, C. Y. (2001). *Macromolecules*, *34*, 6474.